Spatiotemporal early warning system for COVID-19 pandemic

Jaya, I. G. N. M.; Andriyana, Y.; Tantular, B.; Krisiani, F.

[Link to publication in University of Groningen/UMCG research database](#)

SPATIOTEMPORAL EARLY WARNING SYSTEM FOR COVID-19 PANDEMIC

I.G.N.M. JAYA[1,*], Y. ANDRIYANA[2], B. TANTULAR[2], F. KRISIANI[3]

[1]Department Statistics, Universitas Padjadjaran, Indonesia and Faculty of Spatial Sciences, Groningen University,

The Netherlands

[2]Department Statistics, Universitas Padjadjaran, Indonesia

[3]Mathematics Department, Parahyangan Catholic University, Indonesia

Abstract: Wuhan, China reported the outbreak of COVID-19 in December 2019. The disease has aggressively spread around the world, including Indonesia. The emergence of COVID-19 has serious implications for public health and socio-economic development worldwide. No country is prepared to face COVID-19. Because of the rapid transmission of COVID-19, the early warning systems (EWS) in each country are not prepared to deal with it. Controlling and preventing COVID-19 transmission in an effective and efficient manner is critical not only for public health, but also for economic sustainability and long-term viability. Consequently, an efficient and effective EWS for COVID-19 is required. The EWS for COVID-19 must be capable of monitoring and forecasting the spatiotemporal transmission of COVID-19. This study demonstrates how an EWS could be a proactive system that would be able to predict the spatiotemporal distribution of COVID-19 and detect its sudden increase in small areas such as cities. Early COVID-19 data in Bandung, Indonesia from 17 March 2020 to 22 June 2020 was used to demonstrate the construction of an effective and efficient EWS using the spatiotemporal model. We observed that the relative risk of COVID-19

fluctuates geographically and temporally, gradually increasing throughout the estimate phase (17 March 2020-22 June 2020) and increasing slightly during the prediction period (23 June–06 July 2020). We discovered that human mobility is a major aspect that must be addressed in order to minimize COVID-19 transmission during the early pandemic phase.

Keywords: Bayesian; Bandung; COVID-19; early warning system; spatiotemporal.

2010 AMS Subject Classification: 93A30.

1. INTRODUCTION

Toward the end of December 2019, the coronavirus (COVID-19) made headlines worldwide. Wuhan, China reported the outbreak of COVID-19 for the first time on 31 December 2019 [1-3]. Due to its rapid global spread, WHO announced COVID-19 to be a pandemic on 11 March 2020 [4]. The outbreak rapidly spread from Wuhan into at least 200 countries during early pandemic [5,6]. COVID-19 infected every country in the world, with no exception. The emergence of COVID-19 has serious implications for public health and socio-economic development worldwide [7]. By the end of June 2020, there have been over 4.3 million confirmed cases of the COVID-19 pandemic and over 290,000 deaths [7].

No country is fully prepared for COVID-19 [8]. WHO issued an alert during the early coronavirus pandemic, but its message was ignored [9]. Most countries believe they are well-prepared to deal with the coronavirus. By contrast, they greatly underestimated COVID-19. As a result, the global health system and economy were almost on the verge of collapsing. Each country's early warning systems (EWS) are unable to respond to the COVID-19 outbreak due to its rapid spread, lack of disease risk information, and less knowledge of geographical evolution [9] According to the WHO, it is still possible to halt coronavirus spread if countries implement robust measures to identify disease early, treat cases, track contacts, and advocate social isolation [9]. Consequently, an efficient and effective surveillance and EWS for COVID-19 is required [10]. EWS is a surveillance system that collect and analysis epidemic or pandemic-prone diseases data to alert public health authorities. It assists countries during times of crisis when their routine public

health surveillance systems are insufficient, disrupted, or non-existent [11,12]. EWS fills temporary gaps while regular systems recover from disasters or crises. Rapid response to epidemic or pandemic is critical, particularly among refugees and displaced people. However, developing such systems for infectious disease epidemic or pandemic has received little attention.

According to UNISDR (2005) [13], an efficient and effective EWS includes four interrelated elements: (i) risk awareness, (ii) monitoring and early warning service, (iii) communication and dissemination, and (iv) response capability (see Figure 1) [13].
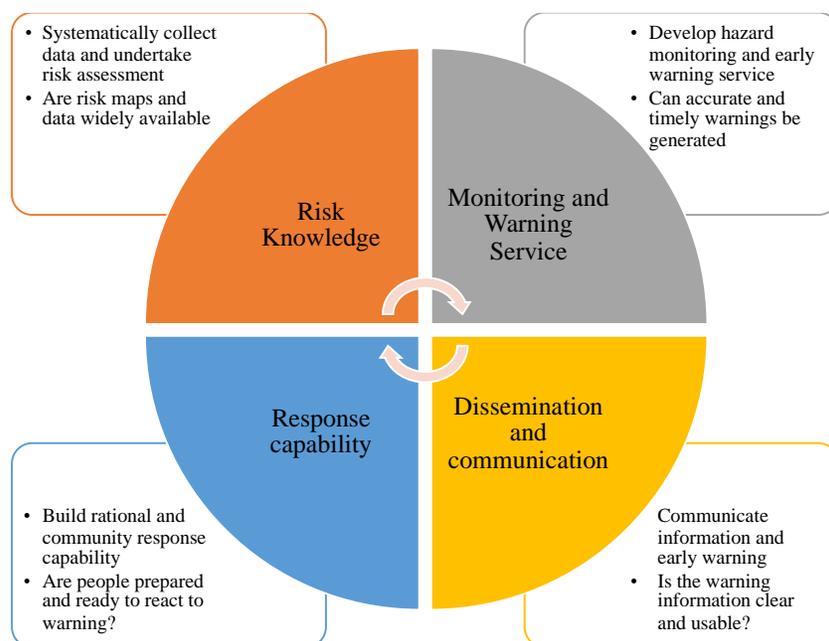
Source: UNISDR (2009)

Figure 1. Four elements of an early warning system

  A failure in any of these elements could cause the system to fail (see [14,15] for detail). The first and second components entail the monitoring and forecasting of the geographic evolution of disease risk in the environment. It has a strong relationship with the statistical model on which we will be concentrating. The EWS for COVID-19 must be capable of monitoring and forecasting the spatiotemporal transmission of COVID-19. It is discussed in this article how an EWS could be a proactive system that would be able to predict the spatiotemporal distribution of COVID-19 and detect its sudden increase.

COVID-19 study is typically conducted in large areas, such as regional areas [16] and countries [17, 18]. There has been very little research conducted on such a small region as a city. COVID-19 will spread more densely in a limited region due to its high level of mobility, which results in a high degree of spatial dependence. Small area characteristics should be taken into account while building an EWS. Additionally, significant risk factors should be identified during the pandemic's early stages. Numerous studies have indicated that human mobility may have an effect on COVID-19 transmission. However, quantifying human movement is fairly difficult [19, 20] and some proxies are required.

The fundamental concept in assessing disease risk in EWS is relative risk. The standard method for calculating relative risk is to divide the number of cases by the expected number of case, called as standardized case ratio (SIR) [21-25]. However SIR provides unreliable estimate of the relative risk for small area with small number of case and population at risk [26-29]. Bayesian smoothing is frequently used to solve the unreliability problem associated with SIR. A hierarchical Bayesian spatiotemporal model is used to smooth, model, forecast, and map disease risk for spatiotemporal data. It provides a reliable estimate of the relative risk over space and time by accounting for spatially and temporally structured and unstructured effects, as well as their interactions [26, 30]. The reliable estimate of relative risk is required for effective and efficient EWS. Additionally, the effectiveness of early intervention techniques remains to be determined by an analysis of available surveillance data.

The purpose of this retrospective analysis is to gain a better understanding of the disease patterns associated with COVID-19 in this region and, as a result, to guide future pandemic response.

The remainder of the paper is divided into the following sections. The next section discusses the materials and methods used in this study. Following that is the Application section, which details the COVID-19 EWS in Bandung, Indonesia. The last part discusses, summarizes, and makes recommendations for additional research.

2. MATERIAL AND METHODS

2.1. Data sources

We use COVID-19 data in Bandung city, Indonesia to demonstrate the construction of an effective and efficient EWS using the spatiotemporal model for small areas and identify the critical risk factors. The COVID-19 dataset was obtained from a website in Bandung that provides real-time information on COVID-19 pandemic disease outbreaks (https://covid19.bandung.go.id/). The website keeps track of newly confirmed cases in Bandung by district and date. Between 17 March 2020 and 22 June 2020, we extensively observed COVID-19 press announcements and situation reports produced by 30 Bandung district health agencies. Because we are dealing with a small area, confirmed cases are extremely rare on a daily basis. As a result, to avoid a large number of zero cases, we take the cumulative cases every week. It is based on COVID-19's incubation period. Symptoms may appear 2-14 days after virus exposure [31]. As proxy measures of human mobility, we used population density and poverty rate. The population at risk, population density and the poverty rate on 2019 were extracted from Bandung Data (https://data.go.id/). Table 1 displays detailed data are used in this study for each district.

Table 1 Data from the Districts in Bandung

id	District	No. Total Cases	Population	Population Density (inhabitants/km²)	Poverty rate (%)[a]
1	Andir	22	87,604	26.33	16.40
2	Antapani	17	92,245	19.67	11.00
3	Arcamanik	13	66,349	11.63	16.40
4	Astanaanyar	17	62,651	23.87	14.70
5	Babakan Ciparay	16	153,417	19.87	21.90
6	Bandung Kidul	6	70,653	9.79	19.60
7	Bandung Kulon	27	146,106	22.18	20.30
8	Bandung Wetan	6	28,374	9.13	9.80
9	Batununggal	9	110,385	24.07	22.00
10	Bojongloa Kaler	20	113,213	39.99	29.40
11	Bojongloa Kidul	8	86,618	13.80	21.10
12	Buah Batu	10	103,406	12.02	17.70
13	Cibeunying Kaler	12	64,925	15.82	13.00
14	Cibeunying Kidul	10	97,755	20.60	15.80
15	Cibiru	16	83,910	11.13	18.70
16	Cicendo	43	99,644	14.56	12.80
17	Cidadap	7	61,916	9.56	12.80
18	Cinambo	3	27,958	6.73	18.80
19	Coblong	22	128,371	17.96	16.20
20	Gedebage	9	38,716	3.75	13.70
21	Kiaracondong	18	127,032	21.59	21.10
22	Lengkong	7	65,901	12.14	11.00
23	Mandalajati	2	76,987	9.47	17.60
24	Panyileukan	5	47,271	7.71	13.60
25	Rancasari	6	81,394	10.30	11.80
25	Regol	20	79,655	19.07	15.90
27	Sukajadi	11	106,940	25.23	17.20
28	Sukasari	4	80,370	13.08	9.40
29	Sumur Bandung	9	32,235	10.56	9.50
30	Ujungberung	9	85,887	11.79	20.40
		384	2,507,888	15.78	16.32

[a]Total number of very poor, poor, near poor vulnerable to poverty household divided by total number of household

2.2 Method

Moran's I

For an effective monitoring and controlling COVID-19, the prior information on spatiotemporal autocorrelation of COVID-19 risk transmission is required [3]. Spatiotemporal Moran's I statistic on case rate is used. It is defined as [24].

$$\text{MoranST} = \frac{nT \sum_{i=1}^{n} \sum_{t=1}^{T} \sum_{j=1}^{n} \sum_{s=1}^{T} \widetilde{w}_{(it,js)} (p_{it} - \bar{p})(p_{js} - \bar{p})}{\sum_{i=1}^{n} \sum_{t=1}^{T} \sum_{j=1}^{n} \sum_{s=1}^{T} \widetilde{w}_{(it,js)} \sum_{i=1}^{n} \sum_{t}^{T} (p_{it} - \bar{p})^2} \tag{1}$$

for $i = 1, .., n$ and $t = 1, ..., T$ with n and T denote the number of districts and total time periods. i and j were district indices indicating the adjacency of districts i and j, $\widetilde{w}_{(it,js)}$ is the weight accounting for the spatiotemporal autocorrelation between p_{it} and p_{js}, defined as:

$$\widetilde{w}_{(it,js)} = \begin{cases} w_{ij} & \text{if } t = s \\ 1 & \text{if } i = j \text{ and } /t - s/ = 1 \\ 0 & \text{otherwise} \end{cases}$$

where w_{ij} is one if regions i and j are neighbours, and zero otherwise. This study considered the queen's adjacency as a spatial weight matrix. p_{it} and p_{jt} denoted the prevalence rate in district i and j over period t, and $\bar{p}$ was the average of the prevalence rate in the entire region over time period. The prevalence rate p_{it} is defined as:

$$p_{it} = \frac{y_{it}}{N_{it}} \times 100.000 \tag{2}$$

where y_{it} and N_{it} denote the number of new cases and population at risk at district i and period t respectively. Zero spatiotemporal Moran's I (MoranST) indicated that the data lacked spatial autocorrelation [32]. A positive spatiotemporal Moran's I value suggested that adjacency values were clustered together, whereas a negative spatiotemporal Moran's I value indicated that different values were clustered together. The high value of spatiotemporal Moran's I reflects the intensity of spatial autocorrelation, indicating that the COVID-19 has been transmitted to surrounding locations over time.

2.3. Bayesian hierarchical spatiotemporal-model

Bayesian hierarchical models have been used often to evaluate spatiotemporal disease transmission

extending [33-35]. It has been successfully to forecast disease risk and monitor the disease transmission [24] which are crucial components in developing EWS. Here we adopt the one defined by Knorr-Held (2000) [36] in which the spatial, temporal and spatiotemporal interaction components are model as random effects. The interaction components were included in the model to consider the variation of temporal trend over districts. The Bandung city is divided becomes n districts over T periods. For the district i in periode t we assume COVID-19 cases y_{it} follows Poisson distribution[1][24]:

$$y_{it} \sim Poisson(\lambda_{it})$$

where λ_{it} denotes the expectation and variance of y_{it} at district i and time t. In order to study of the relative risk, λ_{it} is defiend as a product of expected number of cases (E_{it}) and the relative risk (θ_{it}); $\lambda_{it} = E_{it}\theta_{it}$, $i = 1, \dots, n$ and $t = 1, \dots, T$. The expected number of confirmed case is defined as [24, 25]:

$$E_{it} = N_{it} \frac{\sum_{i=1}^{n} \sum_{t=1}^{T} y_{it}}{\sum_{i=1}^{n} \sum_{it=1}^{T} N_{it}} \quad i = 1, \dots, n \text{ and } t = 1, \dots, T \tag{3}$$

Now we will examine the Poisson distribution's mean, which we will decompose using the natural logarithm link function [24, 25]:

$$\log(\lambda_{it}) = \log(E_{it}) + \log(\theta_{it}) \tag{4}$$

The second component in Eq. (4), $\eta_{it} = \log(\theta_{it})$, is the focus of further research. Specifically:

$$\eta_{it} = \alpha + \omega_i + \nu_i + \phi_t + \gamma_t + \delta_{it} \tag{5}$$

where α is the intercept representing the overall relative risk; ω_i, ν_i, ϕ_t and γ_t are the random effect components that are spatially structured and unstructured effects, and temporally structured and unstructured effects, respectively. δ_{it} is a representation of spatiotemporal of interaction. The random effect of region i (ω_i) is described spatially structured using the intrinsic conditional autoregressive (iCAR) prior [33]:

---

[1]To address the issue of overdispersion that occurs when data contains an excess of zeroes, a negative binomial (NB) distribution [50, 51]　or a　zero-inflated Poisson (ZIP) distribution [52] or a　zero-inflated negative binomial (ZINB) distribution [53].

$$\omega_i | \boldsymbol{\omega}_{-i}, \tau_\omega, \mathbf{W} \sim \mathcal{N} \left(\frac{\sum_{j=1}^n w_{ij} \omega_j}{\sum_{i=1}^n w_{ij}}, \frac{1}{\tau_\omega \sum_{i=1}^n w_{ij}} \right) \tag{6}$$

where $\boldsymbol{\omega}_{-i}$ refers to the elements in $\boldsymbol{\omega}$ except the ith element, $\mathbf{W} = (w_{ij})$ is queen spatial weight matrix. τ_ω is the precision parameter of ω_i. The random effect of region i (v_i) is spatially unstructured and follows an exchangeable normal distribution (i.e. a sequence of random variables that are independently and identically normal distributed) [24, 25]:

$$v_i | \tau_v \sim \mathcal{N} \left(0, \frac{1}{\tau_v} \right) \tag{7}$$

where τ_v is the precision parameter of v_i. A prior for temporal trend (φ_t) is a random walk of order one (RW1) [24]:

$$\varphi_{t+1} - \varphi_t | \tau_\varphi \sim \mathcal{N} \left(0, \frac{1}{\tau_\varphi} \right) \tag{8}$$

with τ_φ being the precision parameter. We may use a random walk of order two (RW2) instead of a RW1. This RW2 priors is commonly used if the data has a pronounced linear trend. The temporal trend (φ_t) of a RW2 is [24, 37]:

$$\varphi_t - 2\varphi_{t+1} + \varphi_{t+2} | \tau_\varphi \sim \mathcal{N} \left(0, \frac{1}{\tau_\varphi} \right) \tag{9}$$

Temporally unstructured effect γ_t is assumed to follows exchangeable normal distribution [24, 25]:

$$\gamma_t | \tau_\gamma \sim \mathcal{N} \left(0, \frac{1}{\tau_\gamma} \right) \tag{10}$$

with τ_γ being the precision parameter of γ_t. The interaction effect δ_{it} follows for different structures I-IV which describe the product of spatially and temporally structured and unstructured effects (see [24, 36] for detail).

We specify a vague Gaussian prior distribution with zero mean and a large variance $\sigma_\alpha^2 = \tau_\alpha^{-1}$ for α, i.e. $\alpha \sim \mathcal{N}(0, 10^6)$ and half Cauchy (HC) prior for hyperparameters. We proposed 25 as scale parameter for the HC hyper-prior. It is possible that not all components in the model (5)

must be included in the model. For the purpose of evaluating our model using deviance information criterion (DIC). The main objective of this paper is to explore the spatiotemporal distribution of COVID-19 and make a relative risk prediction for two weeks ahead. Forecasting with INLA can be easily implemented by imputation missing value scenarios. We can enter 'Not Available (NA)' for the observations that need to be forecasted [38].

For the visual representation of the geographical distribution of COVID-19 we present choropleth maps.

3. APPLICATION: SPATIOTEMPORAL MODELING OF COVID-19 IN BANDUNG CITY, INDONESIA

3.1 Descriptive statistics

As of 22 June 2020, Indonesia had officially confirmed 56,385 cases of COVID-19, including 2,876 deaths. Bandung is the main city of West Java province, which ranks second in terms of COVID-19 cases after Jakarta. In a similar time period, West Java confirmed 2,864 cases. Bandung confirmed 384 cases, representing 13.41 % of all cases in West Java and a prevalence rate of 12.75 cases per 100,000 inhabitants (https://covid19.bandung.go.id/). Figure 2 shows the number of new cases and number of total COVID-19 cases, respectively.
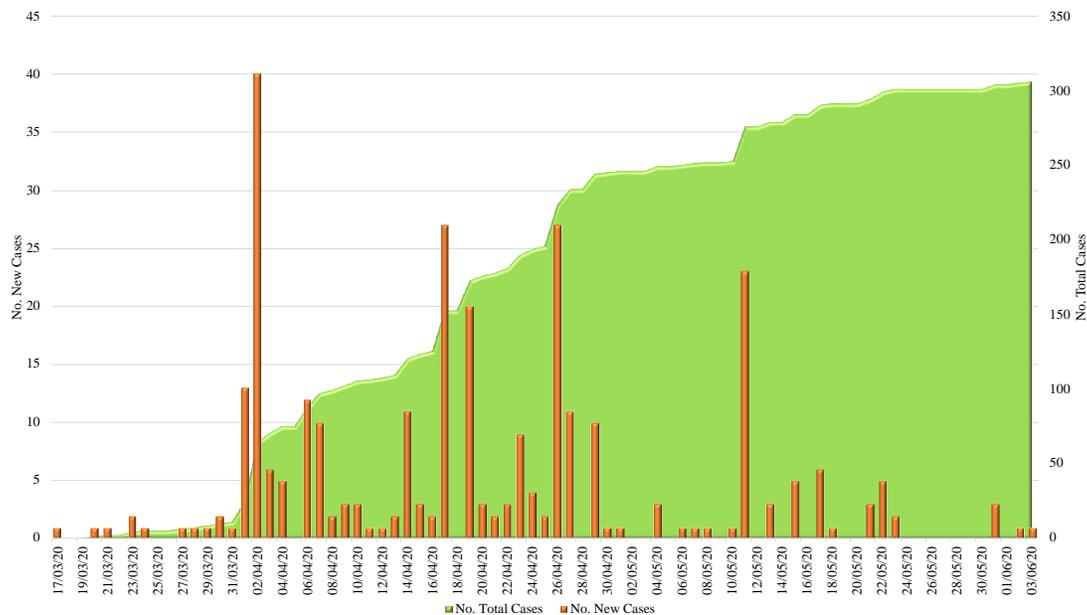

Figure 2. Number of new cases and number of total COVID-19 cases from 17 March to 22 June 2020

Figure 2 shows that a pandemic curve of confirmed cases was no obvious temporal pattern. The number of newly reported instances changes over time. During the early phases of the pandemic, the situation was very modest, with only a few confirmed cases reported daily in Bandung. The greatest spike in new COVID-19 infections occurred on 2 April 2020, when 42 new cases were reported on a single day. This could be due to the fact that the number of tests varies and no preventive actions were provided in early pandemic. The total number of cases follows a significantly nonlinear quadratic pattern, with the added number of new cases being relatively low between 12 May and 22 June 2020.

3.2 Bayesian spatiotemporal model

Preparing to run the spatiotemporal model (5), we calculate the spatiotemporal Moran's I of the COVID-19 case rate. We discovered that the spatiotemporal Moran's I is approximately 0.71(p-value 0.001). This implies that COVID-19 instances are clustered spatially and temporally in Bandung. As a result, the spatiotemporal model is the best candidate for evaluating and forecasting COVID-19 transmission.

We analyze six different sub-models of model (5) that are based on the interaction of spatially and temporally structured and structured effects. By combining four alternative likelihood functions (Poisson, Negative Binomial, Zero Inflated Poisson, and Zero Negative Binomial) with two different priors for temporal trend, the six sub-models were developed into 48 variant sub-models (RW1 and RW2). We use deviance information criterion (DIC), Watanabe Akaike information criterion (WAIC), marginal predictive likelihood (MPL), mean absolute error (MAE), root mean square error (RMSE), and person correlation (r) criteria for selected the best model. The best model should have the smallest DIC, WAIC, MAE, RMSE, and the smallest MPL and r [24].

Table 2. Deviance information criterion (DIC), Watanabe Akaike information criterion (WAIC), marginal predictive likelihood (MPL), mean absolute error (MAE), root mean square error (RMSE), and person correlation (r) criteria[a]

Model	Likelihood	Temporal Structured	DIC	WAIC	MPL	MAE	RMSE	r
M1	P	RW1	894.306	904.922	-453.395	0.668	1.037	0.713
		RW2	893.865	904.671	-453.268	0.668	1.038	0.711
	NB	RW1	890.079	893.046	-447.217	0.674	1.050	0.723
		RW2	889.663	893.361	-447.397	0.673	1.050	0.719
M2	P	RW1	894.710	905.438	-453.693	0.668	1.036	0.718
		RW2	894.607	905.324	-453.627	0.668	1.037	0.717
	NB	RW1	891.070	893.357	-447.437	0.673	1.052	0.739
		RW2	890.885	893.169	-447.282	0.674	1.051	0.727
M3	P	RW1	871.689	874.265	-449.640	0.522	0.750	0.761
		RW2	871.713	874.988	-449.212	0.526	0.757	0.761
	NB	RW1	876.774	880.205	-1998.686	0.552	0.807	0.747
		RW2	875.912	880.078	-8550.494	0.552	0.806	0.745
M4	P	RW1	888.314	896.232	-453.863	0.597	0.879	0.759
		RW2	901.229	906.236	-495.950	0.583	0.845	0.807
	NB	RW1	894.831	896.205	-450.953	0.624	0.944	0.767
		RW2	905.380	904.839	-651.006	0.593	0.870	0.819
M5	P	RW1	885.592	897.924	-457.177	0.580	0.880	0.806
		RW2	877.689	886.150	-450.828	0.564	0.837	0.753
	NB	RW1	891.332	895.722	-451.924	0.596	0.927	0.839
		RW2	881.955	887.460	-447.566	0.585	0.885	0.753
M6	P	RW1	885.481	897.814	-457.122	0.580	0.880	0.806
		RW2	903.376	915.842	-605.881	0.558	0.831	0.861
	NB	RW1	891.451	895.840	-451.984	0.596	0.927	0.839
		RW2	909.597	912.145	-714.508	0.568	0.881	0.916

[a]Due to the limited space, the DIC, WAIC, MPL, MAE, RMSE, and r values for the Zero inflated Poisson and Negative Binomial are available upon request.

P: Poisson

NB: Negative Binomial

RW: Random walk

M1: $\eta_{it} = \alpha + \omega_i + v_i$

M2: $\eta_{it} = \alpha + \omega_i + v_i$

M3: $\eta_{it} = \alpha + \omega_i + v_i + \phi_t + \gamma_t + \delta_{it}$ (Type I)

M4: $\eta_{it} = \alpha + \omega_i + v_i + \phi_t + \gamma_t + \delta_{it}$ (Type II)

M5: $\eta_{it} = \alpha + \omega_i + v_i + \phi_t + \gamma_t + \delta_{it}$ (Type III)

M6: $\eta_{it} = \alpha + \omega_i + v_i + \phi_t + \gamma_t + \delta_{it}$ (Type IV)

Table 2 shows that all of the models M1–M6 variants have a nearly identical value for the model selection criteria. M3 with Poisson probability and RW1 temporal trend, on the other hand, was determined to fit the model selection criterion. It has a low DIC, WAIC, MAE, and RMSE but a high MPL and r. As a result, for the following analysis, we will use this model, which we will refer to as M3. The posterior means of the hyperparameters are presented in Table 3.

Table 3. Posterior mean of the hyperparameter of spatially and temporally structured effects and their interaction

Hyperparameters	Mean	q(0.025)	q(0.975)	Fraction variance (%)
Spatial autoregressive coefficient (ρ)	0.459	0.046	0.890	
Variance of spatially structured effect (σ_ω^2)	0.135	0.033	0.494	4.573
Variance of spatially unstructured effect (σ_v^2)	0.082	0.011	0.358	2.773
Variance of temporally structured effect (σ_ϕ^2)	1.277	0.075	7.738	43.198
Variance of temporally unstructured effect (σ_γ^2)	1.293	0.293	5.443	43.719
Variance of interaction type I effect (σ_δ^2)	0.170	0.063	0.406	5.738

The spatial autoregressive coefficient (ρ) of 0.46 suggests that spatial dependence between adjacent districts is moderate. A random effect's posterior mean of variance quantifies its contribution to the spatiotemporal variation in COVID-19 risk. As shown in Table 3, the posterior means of the random effects' variances range significantly, ranging from 0.082 for the spatially unstructured effect to 1.293 for the temporally unstructured effect's variation. Additionally, Table 3 illustrates the fraction variance of the hyperparameters. The spatiotemporal variance in COVID-19 risk in Bandung is best explained by temporally structured and unstructured effects with total fraction variance is around 86.92%. This shows that there are risk variables that vary over time and play a significant role in COVID-19 transmission, such as human mobility.
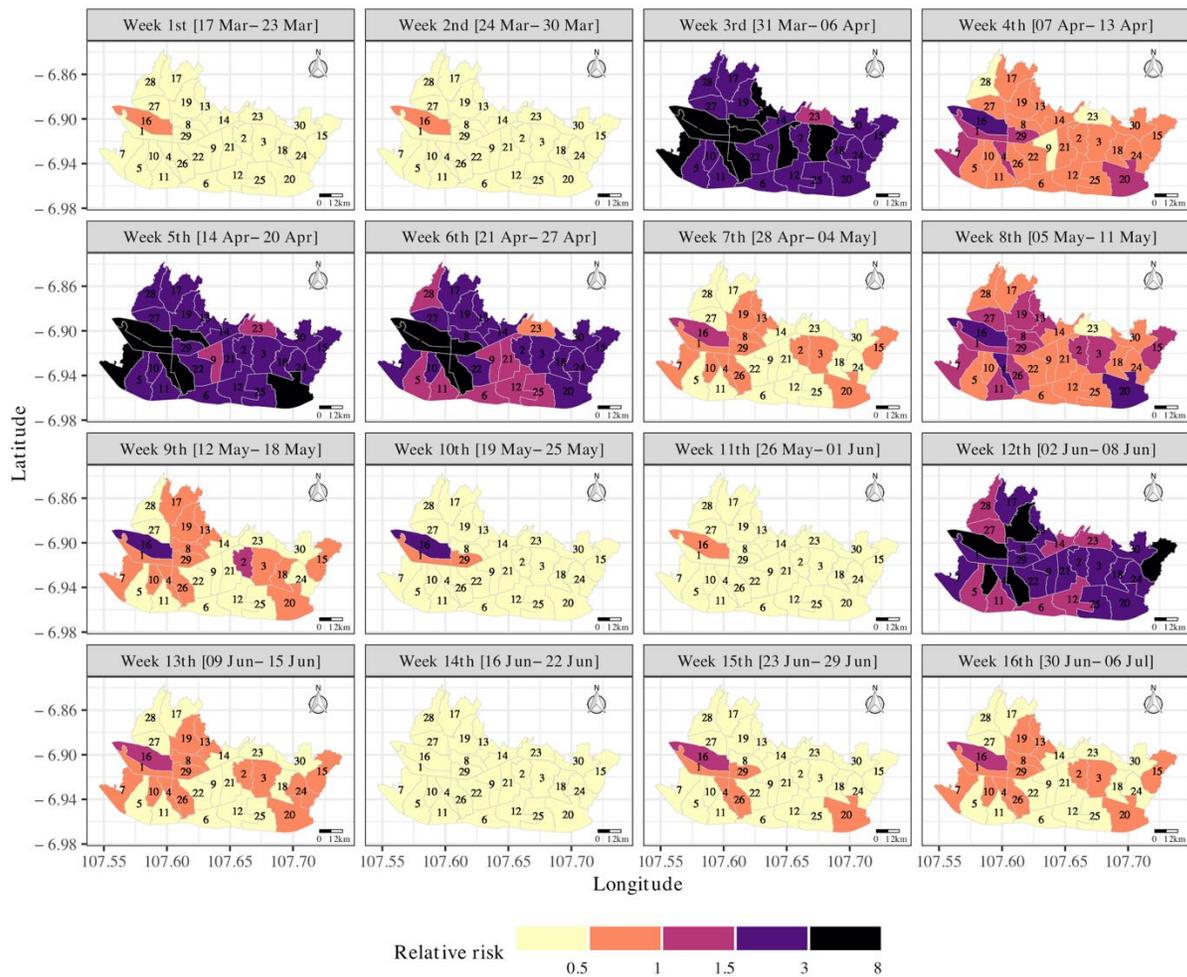

Figure 3. Number of new cases and number of total COVID-19 cases from 17 March to 22 June 2020 (Note: id on the map refers to id in Table 1)

Figure 3 shows the estimated relative risk for weeks 1 to 14 (17 March - 22 June 2020) and the forecasted relative risk for weeks 15 (17 March - 16 June 2020) to 16 (23 Jun -06 Jul 2020). The medium risk was recorded in Cicendo during the first and second weeks (17 March – 30 March 2020). It is possible that this is due to the fact that the Cicendo district is a district with high human movement. In addition, the airport, as well as the train station, are both located in this area.

The COVID-19 showed a considerable increase in the third week (31 Mar – 06 Apr) as the first outbreak. All of the districts have been identified as high-risk regions. Week 4 (07 Apr – 13 Apr) has seen a marked improvement in the situation. However, it was discovered that the number of new cases increased significantly from week 5 (14 Apr – 20 Apr) to week 6 (21 Apr – 27 Apr), which resulted in an increase in the COVID-19 risk. Because of various limitations in human mobility, the number of new cases was somewhat manageable throughout the seventh (28 Apr – 04 May) to eleventh weeks (26 May – 01 Jun). The increase in new cases during week 12 (02 Jun – 08 Jun) results in a significant increase in risk, indicates the second outbreak. During weeks 13 (09 Jun – 15 Jun) and 14 (16 Jun – 22 Jun), the relative risk was less than one in all districts, with the exception of Cicendo district. However, the forecasting period from week 15 (23 Jun – 29 Jun) to week 16 (30 Jun – 06 Jul) indicates that the relative risk of COVID-19 is likely to be higher. Additionally, as illustrated in Figure 3, the Cicendo district is consistently classified as a high-risk area. To determine whether or not the high-risk regions constituted a significant hotspot for COVID-19 risk. We next calculated the exceedance probability $\Pr(\hat{\theta}_{it} > 1|\boldsymbol{y})$.

Figure 4 shows the exceedance probability of estimated and forecasted result of COVID-19 relative risk. In some regions of Bandung, a spatiotemporal relative risk greater than one can be observed with posterior probability more than 0.8, indicating a relatively low level of related uncertainty. In general, the relative risk and associated uncertainty vary significantly by geography. The biggest relative risk is seen in Bandung's western and southeast districts, including Antapani, Astana Anyar, Bandung Wetan, Cicendo, and Gede Bage.
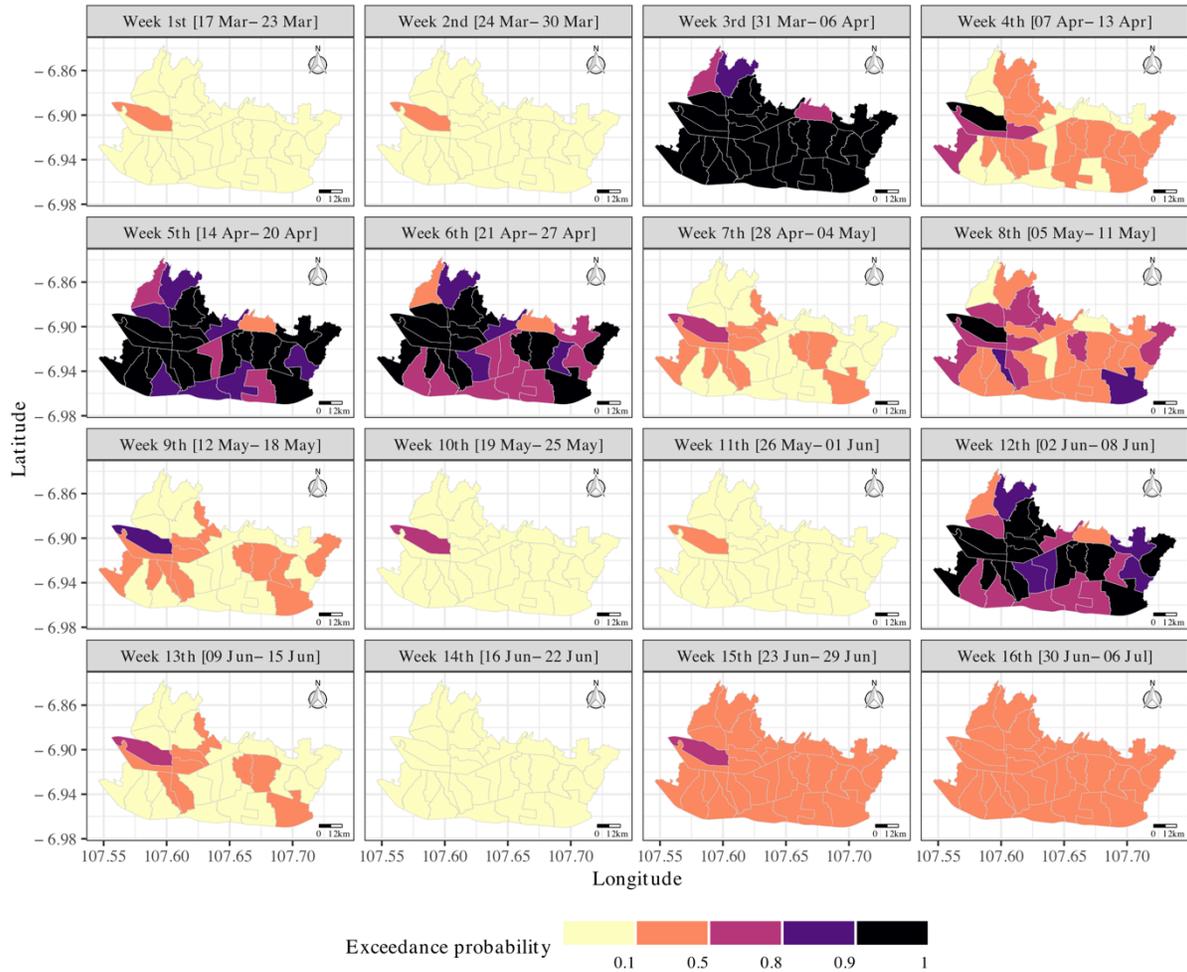
Figure 4. Exceedance probability $\Pr\left(\hat{\theta}_{it} > 1 | \boldsymbol{y}\right)$

The exceedance probability $\Pr\left(\hat{\theta}_{it} > 1 | \boldsymbol{y}\right)$ is depicted in Figure 4. Districts with $\Pr\left(\hat{\theta}_{it} > 1 | \boldsymbol{y}\right)$ more than 0.80 may be classified as high-risk zones or hotspots. Figure 4 demonstrates that during weeks 3, 5, 6, and 12, more than 90% of the districts are classified as high-risk or hotspot. It indicates that during those weeks the number of new cases were significantly increased. Cicendo district has a rather high exceedance probability for the forecast period week 15.
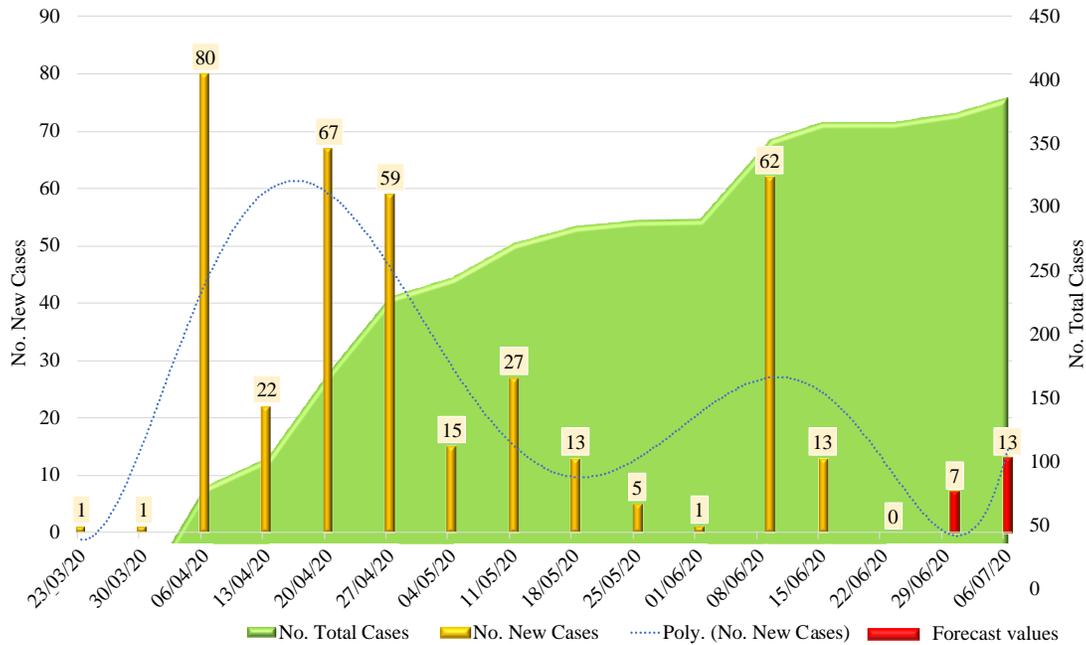
EARLY WARNING SYSTEM FOR COVID-19

Figure 5. Prediction of the number of new cases

Figure 5 illustrates the number of new cases and total cases from 17 March 2020 and 06 July 2020. During the forecast period of 29 June to 06 July 2020, we anticipate an extra 20 cases. In regard to the early warning system, we attempted to identify risk variables that should be controlled in order to prevent the spread of COVID-19. We consider human movement to be the primary risk factor. However, measuring and obtaining human mobility is fairly challenging. According to studies conducted by [39] social mobility is significantly related to population density and poverty. These two variables are used to account for human movement.
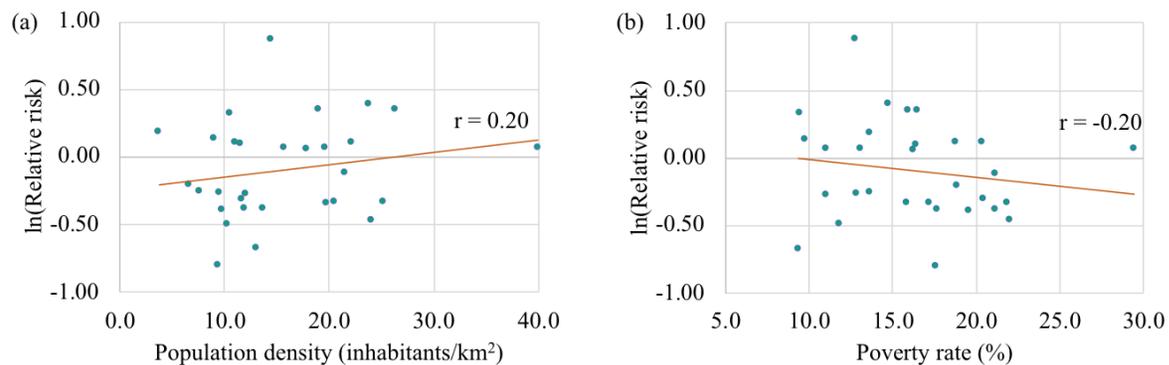

Figure 6. The relationship between population density and poverty rate with the relative risk of COVID-19.

After obtaining COVID-19 forecasts for the next two weeks, we examine the association between population density and poverty rate and estimated of the COVID-19 risk. We done the analysis separately to avoid spatiotemporal confounding problem [25]. We discovered a positive correlation between population density and COVID-19 risk, but a negative correlation between poverty rate and COVID-19 risk. This finding corroborated multiple earlier studies [40]. Human mobility was previously measured by population density and poverty rate. Economic growth is frequently accompanied by an increase in social mobility [39]. In Bandung areas, densely populated places, human mobility is rather high, while it is quite low in impoverished ones. As a result, it is possible to deduce that human movement is a crucial role in COVID-19 transmission [40].

4. DISCUSSION

The mapping and forecasting of diseases are inextricably linked to risk assessment and the EWS warning service. Disease risk mapping has existed in public health and epidemiology for a long period of time [41] Bayesian spatiotemporal disease mapping has been effective in identifying areas at risk [42]. Numerous studies on the COVID-19 pandemic focused on confirmed cases rather than risk factors, oblivious to the fact that the population at risk varies over time and space. It is critical to identify clusters or hotspots of high-risk individuals using the adjusted population at risk. The ratio of observed to expected cases is referred to as the relative risk or excess risk. Not only can spatial and temporal analysis be used to visualize epidemiological data and aid in intuitive disease distribution, but it can also be used to identify spatial and temporal clusters, as well as areas of high and low risk [30]. Using new technologies, GIS analysis, and highly structured mathematical and statistical techniques, the occurrence of infectious diseases can be described and analyzed. Bayesian methods are advantageous for analysing models with complex and flexible structures that accurately represent the characteristics of a particular geographical environment or disease for small area [43].

This is the first study to document the spatiotemporal patterns of the COVID-19 pandemic in Bandung, Indonesia, an area critical for EWS. As a baseline, we used Spatiotemporal Moran's I

statistics on prevalence rates to assess the variation in disease risk spatial dependence over time. To gain a better understanding of the COVID-19 pandemic's spatiotemporal pattern, the Bayesian spatiotemporal model was used to smooth the relative risk of COVID-19 [36]. It is useful for identifying high-risk clusters and forecasting the COVID-19 pandemic relative risk over a one-month period. The Poisson model was found to be superior to the Negative Binomial, Zero inflated Poisson, and Zero inflated Negative Binomial model using DIC, WAIC, MAE, RMSE and Pearson correlation (r). The optimal model included spatially structured and unstructured effects, temporally structured and unstructured effects, and interaction type I. We discovered that the order 1 random walk outperformed the order 2 random walk. To visualize the spatiotemporal pattern of COVID-19 pandemic risk, choropleth maps.

During the second outbreak, COVID-19, new cases were frequently reported in Bandung's southwest and northeast regions. Cases spread to Cicendo's neighboring district, with the queen neighboring district posing an especially high risk of COVID-19 pandemic from the first to ninth periods. The effect eventually spread to all of Bandung's districts. According to Figure 4, the number of new cases has decreased since the tenth period because the Bandung government imposed broad restrictions on people's mobility from May 5 to June 3, 2020, in order to prevent the importation of COVID-19 pandemic cases. Restriction on a large scale is not synonymous with lockdown, during which residents of Bandung are still permitted to travel. It merely restricts the number of visitors from outside Bandung. Local transmission, as a result, remains a viable option. Due to population mobility, the COVID-19 pandemic spread from Cicendo to other districts [44]. This possibility lends credence to the study's discovery of spatial dependency. Using a Bayesian spatiotemporal model, we discovered clear spatiotemporal transmission of the COVID-19 pandemic. The disease spread from Bandung's west to southeast. COVID-19 is extremely likely to spread between geographically neighboring places, according to the results of the examination utilizing geographical neighbourhoods. This could be due to the fact that residents of nearby regions frequently interact. Additionally, the district of Gede Bage in the southeast region, which has a low number of confirmed cases, was designated as a high-risk region due to the district's

small population at risk and a higher than expected number of confirmed cases. When comparing risks across space and time, it is necessary to consider the population at risk, even more so when the population at risk varies significantly across space and time. Additionally, we discovered that human mobility, as defined by population density and poverty rate, is a crucial component in COVID-19 transmission during the early pandemic.

Two additional risk enhancements are visually identified as high-risk clusters in Bandung's western and south-eastern regions on the choropleth map. Due to a physician shortage and a lack of hospital and health center beds, the Bandung government should prioritize clusters at high risk. This data can be used to develop a highly effective and efficient early warning system for COVID-19 transmission control. Bandung's government should place a greater emphasis on high-risk clusters, allocate additional resources to high-risk areas, and implement health protocols such as mask use, social distancing, hand washing, and avoiding crowded areas with limit the human mobility. Human mobility can be restricted by enforcing local lockdowns in locations regarded as hotspots.

5. CONCLUSION

The COVID-19 pandemic is the century's most extraordinary health problem and the greatest threat to humanity since the Second World War. It is rapidly spreading throughout the world, as Wuhan, China reported an outbreak on 30 December 2019 [3]. On 1 March 2020, the WHO declared COVID-19 to be a pandemic. As of 5 June 2020, the coronavirus COVID-19 was present in 213 countries and territories worldwide, as well as on two international transports [5].

This study demonstrates the COVID-19 pandemic in Bandung, Indonesia, on a small spatiotemporal scale. In small regions such as Bandung, the COVID-19 pandemic spread rapidly from district to district despite the government's policy of restricting people's mobility. Examining the spatiotemporal spread is critical to preventing the local transmission and second wave from increasing. This is believed to be the first study to examine the virus's spatiotemporal transmission using a combination of Moran's I and Bayesian spatiotemporal models. The forecasting outcome

can be used to develop a robust early warning system.

Future research, such as an examination of the spatiotemporal distribution of this disease based on demography, hereditary disease, and patient age, will aid in its control and prevention. Through this work, it will be possible to ascertain the factors that influence death and recovery. The Bayesian spatiotemporal model can be used to account for covariates and to control heterogeneity [45, 46].

ACKNOWLEDGMENT

CONFLICT OF INTERESTS

The author(s) declare that there is no conflict of interests.

REFERENCES

[1] H. Zhu, L. Wei, P. Niu, The novel coronavirus outbreak in Wuhan, China, Glob. Health Res. Policy. 5 (2020), 6.

[2] B. Mohan, N. Vinod, COVID-19: an insight into SARS-CoV-2 pandemic originated at Wuhan City in Hubei Province of China, J. Infect. Dis. Epidemiol. 6 (2020), 146.

[3] D. Kang, H. Choi, J.-H. Kim, J. Choi, Spatial epidemic dynamics of the COVID-19 outbreak in China, Int. J. Infect. Dis. 94 (2020), 96-102.

[4] WHO, WHO Director-General's opening remarks at the media briefing on COVID-19 - 11 March 2020, 11 March 2020. [Online]. Available: https://www.who.int/director-general/speeches/detail/who-director-general-s-opening-remarks-at-the-media-briefing-on-covid-19---11-march-2020. [Accessed 12 June 2021].

[5] WHO, Coronavirus disease (COVID-19) advice for the public, WHO, 29 April 2020. [Online]. Available: https://www.who.int/emergencies/diseases/novel-coronavirus-2019/advice-for-public. [Accessed 29 June 2020].

[6] WHO, WHO Director-General opening remarks at the Member State Briefing on the COVID-19 pandemic evaluation - 9 July 2020, 9 July 2020. [Online]. Available: https://www.who.int/director-general/speeches/detail/who-director-general-opening-remarks-at-the-member-state-briefing-on-the-covid-19-pandemic-evaluation---9-july-2020. [Accessed 8 September 2021].

[7] M. Nicola, Z. Alsafi, C. Sohrabi, A. Kerwan, A. Al-Jabir, C. Iosifidis, M. Agha and R. Agha, The socio-economic implications of the coronavirus pandemic (COVID-19): A review, Int. J. Surgery, 78 (2020), 185-193.

[8] M. L. Page, Coronavirus: How well prepared are countries for a covid-19 pandemic? Read more: https://www.newscientist.com/article/mg24532693-500-coronavirus-how-well-prepared-are-countries-for-a-covid-19-pandemic," NewScientist, 12 February 2020. [Online]. Available: https://www.newscientist.com/article/mg24532693-500-coronavirus-how-well-prepared-are-countries-for-a-covid-19-pandemic/. [Accessed 9 September 2021].

[9] A. Maxmen, Why did the world's pandemic warning system fail for COVID? Nature, 589 (2021), 499-500.

[10] WHO, COVID-19 strategy update, WHO, Geneva, 2020.

[11] WHO, EWARN, WHO, 2007. [Online]. Available: http://www.emro.who.int/content/Page-50.html. [Accessed 09 September 2021].

[12] F. Dureab, K. Ahmed, C. Beiersm, C. J. Standley, A. Alwaleedi and A. Jahn, Assessment of electronic disease early warning system for improved disease surveillance and outbreak response in Yemen, BMC Public Health, 20 (2020), 1422.

[13] UNISDR, Terminology on disaster risk reduction, United Nations International Strategy for Disaster Reduction, Geneva, 2009.

[14] J. Zschau, A. N. Kiippers, Early warning systems for natural disaster reduction, Springer, New York, 2003.

[15] N. R. Council, Under the weather: climate, ecosystems, and infectious disease, National Academy Press, Washington, 2001.

[16] M. Zhu, J. Kleepbua, Z. Guan, S. P. Chew, J. W. Tan, J. Shen, N. Latthitham, J. Hu, J. X. Law and L. Li, Early spatiotemporal patterns and population characteristics of the COVID-19 pandemic in southeast Asia, Healthcare, 9 (2021), 1220.

[17] D. Giuliani, M. M. Dickson, G. Espa, F. Santi, Modelling and predicting the spatio-temporal spread of COVID-19 in Italy, BMC Infect. Dis. 20 (2020), 700.

[18] E. Falcão de Oliveira, A.G. de Oliveira, C.C.P. de Arruda, W. de S. Fernandes, M.J. de Medeiros, Spatio-temporal modeling of visceral leishmaniasis in Midwest Brazil: An ecological study of 18-years data (2001–2018), PLoS ONE. 15 (2020), e0240218.

[19] E. T. C. Chagas, P. H. Barros, I. Cardoso-Pereira, et al. Effects of population mobility on the COVID-19 spread in Brazil, PLoS ONE, 16 (2020), e0260610.

[20] J.L. Kephart, X. Delclòs-Alió, D.A. Rodríguez, et al. The effect of population mobility on COVID-19 incidence in 314 Latin American cities: a longitudinal ecological study with mobile phone location data, The Lancet Digital Health. 3 (2021), e716–e722.

[21] D.A. Martínez-Bello, A. López-Quílez, A. Torres-Prieto, Bayesian dynamic modeling of time series of dengue disease case counts, PLoS Negl Trop Dis. 11 (2017), e0005696.

[22] D.A. Martínez-Bello, A. López-Quílez, A. Torres Prieto, Relative risk estimation of dengue disease at small spatial scale, Int. J. Health Geogr. 16 (2017), 31.

[23] I.G.N.M. Jaya, H. Folmer, B.N. Ruchjana, F. Kristiani, Y. Andriyana, Modeling of infectious diseases: a core research topic for the next hundred years, in: R. Jackson, P. Schaeffer (Eds.), Regional Research Frontiers - Vol. 2, Springer International Publishing, Cham, 2017: pp. 239–255.

[24] I.G.N.M. Jaya, H. Folmer, Bayesian spatiotemporal mapping of relative dengue disease risk in Bandung, Indonesia, J. Geogr. Syst. 22 (2020), 105–142.

[25] I.G.N.M. Jaya, H. Folmer, Bayesian spatiotemporal forecasting and mapping of COVID-19 risk with application to West Java Province, Indonesia, J. Regional Sci. 61 (2021), 849–881.

[26] P. Yin, L. Mu, M. Madden, J.E. Vena, Hierarchical Bayesian modeling of spatio-temporal patterns of lung cancer incidence risk in Georgia, USA: 2000–2007, J. Geogr. Syst. 16 (2014), 387–407.

[27] J. Wakefield, Disease mapping and spatial regression with count data, Biostatistics. 8 (2007), 158–183.

[28] D. Clayton, J. Kaldor, Empirical bayes estimates of age-standardized relative risks for use in disease mapping, Biometrics. 43 (1987), 671.

[29] D. Pringle, Mapping disease risk estimates based on small numbers: an assesment of empirical bayes techniques, Econ. Soc. Rev. 27 (1996), 341-363.

[30] G. Yu, R. Yang, Y. Wei, D. Yu, et al. Spatial, temporal, and spatiotemporal analysis of mumps in Guangxi Province, China, 2005–2016, BMC Infect. Dis. 18 (2018), 360.

[31] CDC, Symptoms of COVID-19, 21 February 2021. [Online]. Available: https://www.cdc.gov/coronavirus/2019-ncov/symptoms-testing/symptoms.html. [Accessed 24 September 2021].

[32] P.A.P. Moran, Notes on continuous stochastic phenomena, Biometrika, 37 (1950), 17-23.

[33] J. Besag, J. York, A. Mollie, Bayesian image restoration, with two applications in spatial statistics, Ann. Inst. Stat. Math. 43 (1991), 1–20.

[34] A. Lawson, Statistical methods in spatial epidemiology, John Wiley & Sons, London, 2006.

[35] M. A. Martinez-Beneito and P. Botella-Rocamora, Disease mapping from foundations to multidimensional modeling, CRC Press, Boca Raton, 2019.

[36] L. Knorr-Held, Bayesian modelling of inseparable space-time variation in disease risk, Stat. Med. 19 (2000), 15-30.

[37] I.G.N.M. Jaya, H. Folmer, Identifying spatiotemporal clusters by means of agglomerative hierarchical clustering and Bayesian regression analysis with spatiotemporally varying coefficients: methodology and application to dengue disease in Bandung, Indonesia, Geogr. Anal. 53 (2021), 767–817.

[38] X. Wang, Y.R. Yue, J.J. Faraway, Bayesian regression modeling with INLA, Taylor & Francis, Boca Raton, 2018.

[39] Y. Liu, F. Yamauchi, Population density, migration, and the returns to human capital and land: Insights from Indonesia, Food Policy. 48 (2014), 182–193.

[40] Md.Z. Alam, Is population density a risk factor for communicable diseases like COVID-19? a case of Bangladesh, Asia Pac. J. Public Health. 33 (2021), 949–950.

[41] T. Koch, Cartographies of disease: maps, mapping, and medicine, ESRI Press, Redlands, 2005.

[42] S. Coly, M. Garrido, D. Abrial, A.-F. Yao, Bayesian hierarchical models for disease mapping applied to contagious pathologies, PLoS ONE. 16 (2021), e0222898.

[43] A. López-Quílez, Spatio-temporal analysis of infectious diseases, Int. J. Environ. Res. Public Health. 16 (2019), 669.

[44] W. Zhao, M.A.K. Khalil, The relationship between precipitation and temperature over the contiguous United States, J. Climate. 6 (1993), 1232–1236.

[45] I.G.N.M. Jaya, F. Kristiani, Y. Andriyana, B.N. Ruchjana, Modeling dengue disease transmission for juvenile in Bandung, Indonesia, Commun. Math. Biol. Neurosci., 2021 (2021), Article ID 23.

[46] N. Sunengsih, I.G.N.M. Jaya, A Bayesian spatiotemporal autoregressive model with constant and temporally varying coefficients: an application to hotspot detection of childhood tuberculosis in Bandung City, Indonesia, Commun. Math. Biol. Neurosci., 2021 (2021), Article ID 58.

[47] R. Berk, J.M. MacDonald, Overdispersion and Poisson regression, J. Quant. Criminol. 24 (2008), 269–284.

[48] E.H. Payne, J.W. Hardin, L.E. Egede, V. Ramakrishnan, A. Selassie, M. Gebregziabher, Approaches for dealing with various sources of overdispersion in modeling count data: Scale adjustment versus modeling, Stat. Methods Med. Res. 26 (2017), 1802–1823.

[49] J.D. Lewsey, W.M. Thomson, The utility of the zero-inflated Poisson and zero-inflated negative binomial models: a case study of cross-sectional and longitudinal DMF data examining the effect of socio-economic status, Commun. Dent. Oral Epidemiol. 32 (2004), 183–189.

[50] D. K. Agarwal, A. E. Gelfand and S. Citron-Pousty, Zero-inflated models with application to spatial count data, Environ. Ecol. Stat. 9 (2002), 341–355.